Journal of the Meteorological Society of Japan, Vol. 90, No. 5, pp. 755−770, 2012
DOI: 10.2151/jmsj.2012-512

A Modeling Study on Tropical Cyclone Structural Changes in Response to Ambient Moisture Variations

Yue YING and Qinghong ZHANG

Laboratory for Climate and Ocean-Atmosphere Studies, Department of Atmospheric and Oceanic Sciences, School of Physics, Peking University, Beijing China

(Manuscript received 17 September 2011, in final form 8 May 2012)

Abstract

Recent studies have emphasized the important role of moisture in altering tropical cyclone (TC) vortex structure. Latent heat released in outer rainbands induces change in the secondary circulation, and exerts negative impact on TC inner core intensity. This study is to further explore the TC structural behavior with the presence of vertical wind shear. Typhoon Talim (2005) was simulated using the Weather Research and Forecasting (WRF) model, and sensitivity experiments were conducted by artificially modifying the amount and distribution of moisture around TC vortex. With the presence of an easterly vertical wind shear, the simulated Typhoon Talim developed quasi-stationary outer rainbands that concentrate in the southwestern (downshear left) sector. Air from the north (upstream side of the outer rainbands) traveled faster into TC core than air from the other directions, thus Typhoon Talim was more sensitive to moisture variations in the north than in the south. With enhanced moisture supply into outer rainbands, simulated TCs grow larger in size. However, their inner core intensity and strength are weakened because latent heat released in outer rainbands induces updrafts and reduces mid- to low-level radial inflow that advects absolute angular momentum into inner core. On the contrary, TCs simulated with reduced moisture supply become smaller in size since drier environment inhibits convection in outer core region. The relatively convection-free outer core region favors the formation of strong radial inflow that accelerates the inner core spin-up process. This causes TCs to contract while their inner core strength and intensity increase. Although moisture in outer core region imposes a negative effect on inner core intensification, it contributes to the maintenance of outer core strength and TC size by inducing more convection in the outer core region. Thus, abundant moisture supply in TC outer core region is critical to the growth of horizontal extent of TC primary circulation.

1. Introduction

Condensational heating of moisture from the tropical ocean surface is considered to be the major energy source maintaining the strong rotational wind field of a tropical cyclone (TC) (Emanuel et al. 1994). Relatively high sea surface temperature (SST) and mid-level relative humidity (RH) are the favorable thermodynamic conditions for TCs to intensify because a warmer ocean converts more energy into TC kinetic energy (Elsner et al. 2008). Recently, Hendricks et al. (2010) showed in their composite analysis that, in the West Pacific Ocean, weakening TCs (defined as 24-hour decrease in maximum wind speed more than 6.5 m s^{-1}) displayed lower ambient RH than intensifying TCs. They showed that drier air in the low level wraps into TC core from the northwest periphery. In the Atlantic Ocean, dry air from the Saharan Air Layer intruding into TC core is considered a negative impact on TC intensity (Braun 2010).

However, some researchers showed that the transient response of TC intensity to environmental RH change is different from the aforementioned results because dynamic adjustment of the TC vortex structure could delay the environmental influences (Kimball 2006;

Corresponding author: Qinghong Zhang, Department of Atmospheric and Oceanic Sciences, School of Physics, Peking University, Beijing 100871, China
E-mail: qzhang@pku.edu.cn

Hill and Lackmann 2009). The transient TC behavior brings difficulty to forecasters, who would like to accurately predict TC intensity change just hours before landfall. Kimball (2006) revealed in her modeling study that TC with higher ambient RH develops more rainband convection, which exerts negative impacts on TC intensification by bringing down mid-level low equivalent potential temperature (theta-e) air into the inflow layer. The resulting TC will have a reduced intensification rate in the short-term perspective. But, since the rainband also act as barriers preventing dry air from intruding into the core region, TC with more rainband convection might instead intensify for a longer period of time. To further explain TC's transient response in different thermodynamic conditions, Wang (2009) performed a set of numerical experiments concerning TC structural changes in response to different rainband diabatic heating and cooling rates. He proposed that TC with larger diabatic heating rate in the outer spiral rainbands will expand and weaken. The results showed that pressure dropped more on the inward side of rainbands because of the greater inertial stability there. Thus, an increased diabatic heating rate yields reduced pressure gradient and results in a weakening TC. The experiments by Hill and Lackmann (2009) verified these results in the potential vorticity (PV) framework. They deduced that the lateral extent of wind field (TC size) is related to the PV growth due to latent heat released in outer rainbands.

As was proposed by Holland and Merrill (1984), TC vortices could vary not only in maximum wind speed (intensity), but also in the extent of wind field (size and strength). In Fig. 1 we plot the intensity-size diagram for west Pacific TCs during 2003~2010. It is clear that, for large TCs (with size over 200 km), the intensity and size are not well correlated. Some TCs may intensify while their size is decreasing, and some may have continuously increasing size while intensity remains unchanged. Thus, better prediction of TC structural change is needed for the short-term intensity forecast.

The prediction of TC structural changes is even more complicated in the real atmosphere because TCs often develop asymmetric rainband convection and vortex structure (Lonfat et al. 2004). The main cause of such asymmetries is the vertically changing storm relative flow, namely vertical wind shear that displaces vortices on each level (Wang and Holland 1996). They showed that convection was enhanced to the downshear left of the TC center. Such vertical shear-induced asymmetry was also found by Frank and Ritchie (2001) in model simulation and by Heymsfield et al. (2006) in observation. Most recently, Riemer and Montgomery

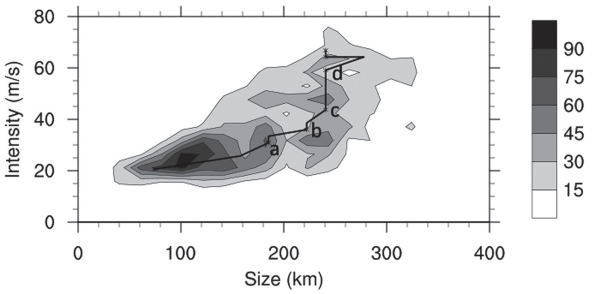

Fig. 1. Number of occurrence (shadings) of size and intensity of Northwest Pacific TCs during 2003~2010. Intensity is defined as maximum sustained low level wind speed, and size as radius of gale-force wind (17 m s^{-1}). Both intensity and size were calculated using JTWC best track data. The structural evolution path of Typhoon Talim (2005) during its developing period is shown as a black line. Typhoon Talim experienced a size-growth period (point **a** to **b** as 00~12UTC, August 29), followed by an intensification period (point **c** to **d** as 00~12UTC, August 30).

(2011) showed with their simple kinematic model of TC-environment interaction that vertical wind shear modifies the pathway of environmental air reaching TC core. They indicate that the TC's interaction with asymmetric dry or moist environmental air could result in different intensity changes depending on the shear direction.

The purpose of this study is to explore the behavior of TC vortices with the presence of asymmetries induced by vertical wind shear. In addition to previous idealized experiment results (Wang 2009; Hill and Lackmann 2009), we believe our experiments with more realistic TC circulation could draw a more detailed picture of TC's interaction with ambient moisture. Typhoon Talim (2005) in Northwestern Pacific is selected as a real case for numerical experiments, and its ambient moisture field is artificially modified. The resulting TC structural changes in response to such ambient moisture perturbations are analyzed.

In Section 2, we briefly describe the data, configuration of numerical model and the design of sensitivity experiments. Section 3 will provide the model simulation results and interpretations of these results will be presented in Section 4. Section 5 will draw conclusion and raise several issues concerning possible further studies.

2. Data description and experimental design

The structural evolution path of Typhoon Talim (2005) during its developing period is printed on Fig. 1 according to the 6-hourly records from JTWC best track data (Atangan and Preble 2006). We selected Typhoon Talim as a real case for this study because its life cycle somewhat represents the average of all West Pacific typhoons during 2003~2010. The developing period of Typhoon Talim can be divided into two stages: the size-growth period before 12UTC 29 August and the intensification period after 00UTC 30 August.

We employed the Weather Research and Forecast (WRF) model version 3.2.1 to conduct numerical experiments. The model was setup up with one single domain with 4 km grid spacing, 400 × 600 grid points in the horizontal and 26 σ levels in the vertical. The moist convection processes are simulated explicitly with WRF Single-Moment 6-class (WSM6) microphysics scheme (Hong and Lim 2006). Planetary boundary layer and surface processes are simulated with Yonsei University scheme (Hong et al. 2011). Longwave and shortwave radiations are simulated with Rapid Radiative Transfer Model (RRTM) (Mlawer et al. 1997) and Dudhia scheme (Dudhia 1989), respectively. Initial conditions and realistic boundary conditions were provided by final analysis data from National Centers for Environmental Prediction (NCEP final analysis). A symmetric bogus Rankine vortex (Low-Nam and Davis 2001) was inserted as the initial model TC vortex. The vortex location and maximum wind speed was specified in accordance with the best track data from Joint Typhoon Warning Center (JTWC). Due to the imbalance between bogus vortex and model initial synoptic fields, a 24-hour period of spin-up integration was performed to derive a relatively balanced and mature-stage TC vortex. All simulations started at 00UTC 28 August and ended at 12UTC 30 August.

In order to evaluate TC structural changes in response to ambient moisture amount and distribution, a series of sensitivity experiments were conducted by artificially modifying model water vapor mixing ratio (*qv*) fields. Table 1 explains the modification of *qv* in each experiment. The modification of *qv* was made at 00UTC 29 August, and they were applied to the model grid from surface to 3.5 km in the vertical and 300 km away from TC center in the horizontal. Lateral boundary fluxes were also modified in accord with adjacent grid points to ensure consistency. Linear interpolation was performed along borders to prevent abrupt changes in the field. In the next section, we will evaluate TC vortex evolution in the 36-hour periods (designated as t = 0~36h) after the modifications took place. The size-growth period and intensification period hereafter refer to t = 0~24h and t = 24~36h, respectively.

Table 1. Modification of water vapor mixing ratio (*qv*) in experiments.

Exp. name	Description
Ctrl	Control experiment
Q-	Subtract 2 g kg^{-1} of *qv*
Q+	Add 2 g kg^{-1} of *qv*
QN-	Subtract 2 g kg^{-1} of *qv* from northern sector
QS-	Subtract 2 g kg^{-1} of *qv* from southern sector
QN+	Add 2 g kg^{-1} of *qv* to northern sector
QS+	Add 2 g kg^{-1} of *qv* to southern sector

3. Simulation results

3.1 Asymmetries in simulated TCs

The simulated TCs display evident asymmetries in both rainband convection and wind field structure. Storm-relative flow was calculated by averaging wind within 200km<r<600km area. In CTRL, the storm-relative flow and radar reflectivity at surface, 3km and 9km height are shown in Fig. 2. During the size-growth period, the storm-relative flow on each level were mostly westerlies. As the intensification period starts, the storm-relative flow vary on each level and an easterly vertical wind shear forms (see the shear vector in CTRL, 36h in Fig. 3). A convergence line forms at surface in the western sector near TC center, where high theta-e air from the northeast met with low theta-e air from the northwest (Fig. 4). The convergence line favors uplifting of high theta-e air, thus rainband convection is concentrated in the southwestern sector of TC. This shear-induced flow pattern closely resembles the observed wind field structure of tropical storm Chantal (Heymsfield et al. 2006). The down-shear left preference of rainband convection also agreed with previous statistical studies (Corbosiero and Molinari 2002).

For all runs, TCs develop easterly vertical wind shear during their intensification period (Fig. 3). Their outer spiral rainbands are all concentrated in the southwestern sector. However, compared with CTRL, TCs in Q- and QN- are smaller in size and have fewer outer rainbands. From the distribution of horizontal wind speed (Fig. 5), we can deduce that wind field structure of Q- and QN- are much more axi-symmetric than that of CTRL. For CTRL, QS-, QN+, QS+ and Q+, wind

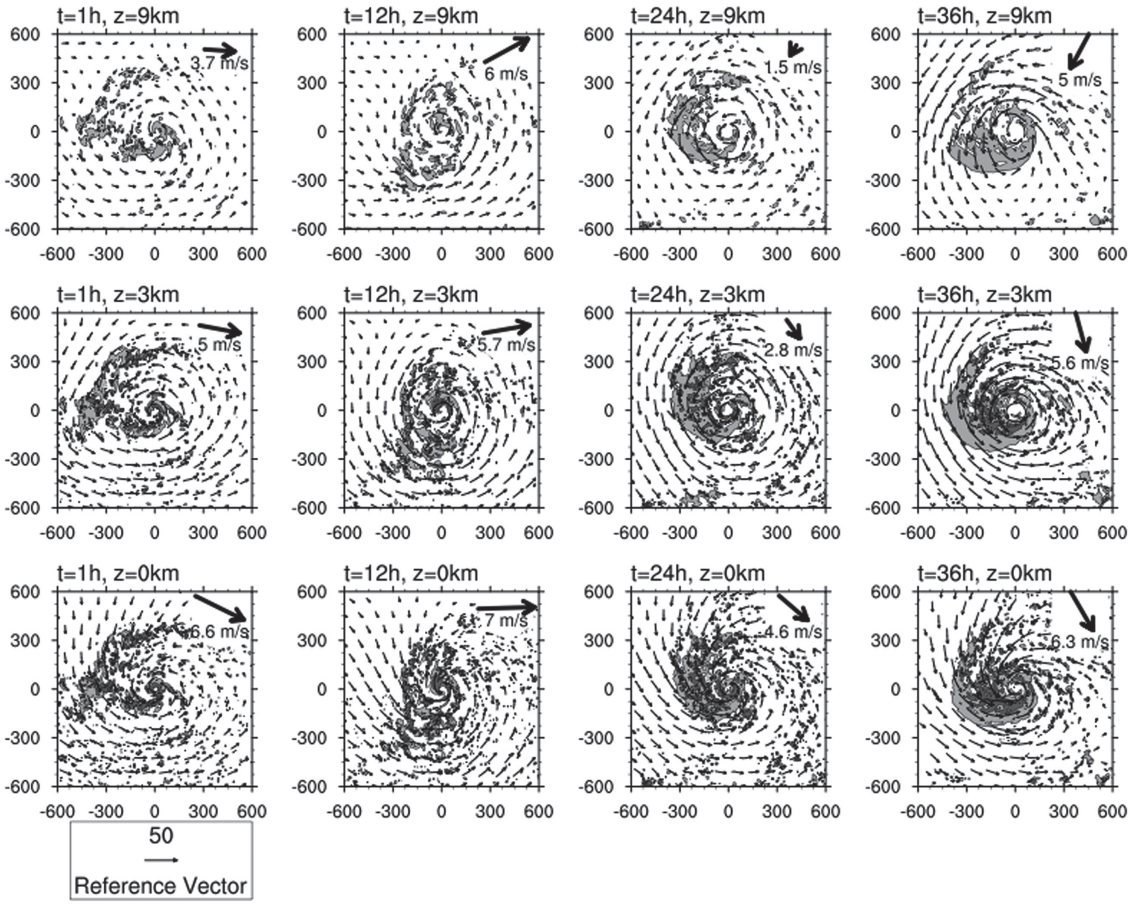

Fig. 2. Plane view of horizontal wind fields relative to TC center in CTRL run. Wind fields are shown at z = 0, 3 and 9 km (from bottom up) and at t = 1, 12, 24 and 36h (from left to right). The radar reflectivity of the corresponding level and time are shown in shadings (20~40dBZ in light gray and 40~60dBZ in dark gray). Storm-relative flow is calculated by averaging wind within 200 km < r < 600 km area, and is shown on the upper-right corner of each plot (magnitude in m s^{-1} is shown below each vector). The difference of upper- and low-level storm-relative flow is equivalent in definition with the vertical wind shear imposed on TC circulation. The horizontal scale is distance (km) from TC center.

speed maxima appear in the southern sector near TC core.

3.2 Wind field parameters

To get a more detailed view of TC structural changes, we need to find parameters describing the peak and spread of wind field. Following the definition of TC intensity, strength and size by Holland and Merrill (1984), we calculated these parameters using simulated TC wind field at 1 km height, where horizontal wind speed maxima are found in the vertical. In CTRL, TC developed a secondary wind speed maximum at ~150km radius outside the primary eyewall during its intensification period (Fig. 5). TC eyewall and inner rainbands are well enclosed by 100-km radius, while the bulk of outer rainband convection is located outside of 100-km radius. We thus define TC inner core as the area within 100km radius and TC outer core as the annulus area within 100<r<300 km. The traditional way of calculating TC intensity is to search for tangential wind maximum within the whole TC circulation. In this paper, instead of showing the shift in radius of maximum wind, we calculated wind speed maxima (intensity) in both inner and outer core regions in order to monitor their strengthening and weakening separately. We define TC size as radius of gale force

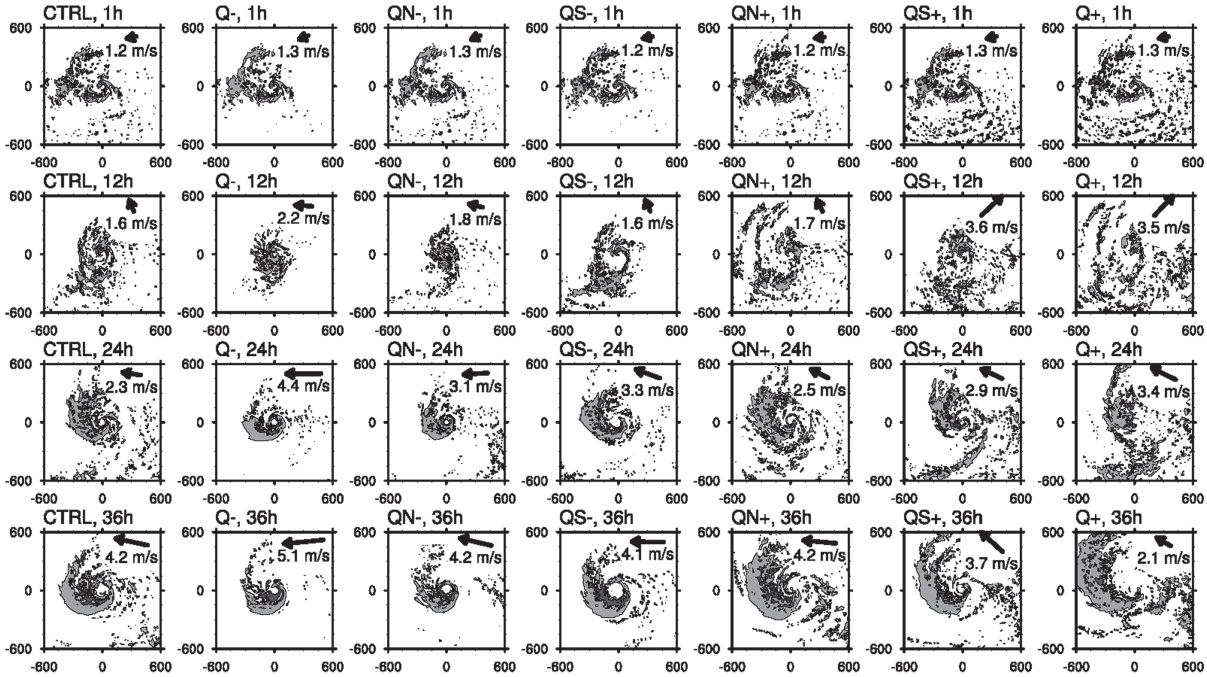

Fig. 3. Plane view of radar reflectivity at 3 km height for each run (CTRL, Q-, QN-, QS-, QN+, QS+ and Q+ from left to right) at t = 1, 12, 24 and 36 h (from top to bottom). Radar reflectivity is shown in shadings (20~40dBZ in light gray and 40~60dBZ in dark gray). A shear vector is drawn on the upper right corner of each plot, and the magnitudes of vertical shear (in m s^{-1}) are shown below the vector. The vertical wind shear is defined as the difference of storm-relative wind at z = 9 km and z = 3 km. The horizontal scale is the distance (km) from TC center.

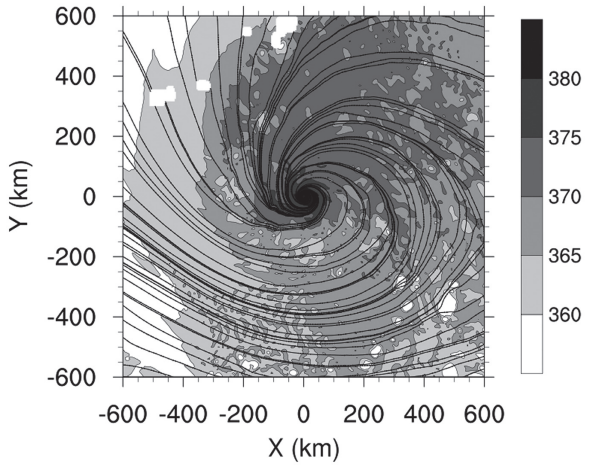

Fig. 4. Surface wind field (streamline) and equivalent potential temperature (shadings for 360~380 K) simulated at t = 30h in CTRL. X and Y axes are distance (km) from TC center.

wind (17 m s^{-1}) and the inner (outer) core strength as the relative angular momentum averaged over inner (outer) core.

Figure 6 shows the evolution of aforementioned TC wind field parameters. In CTRL, TC inner core intensity (Fig. 6a) reached 44 m s^{-1} at t = 18h, but decreased to 35 m s^{-1} before the intensification period started. The outer core intensity (Fig. 6b) increased gradually from 20 m s^{-1} to 30 m s^{-1} during the size-growth period, and when the intensification period started, the outer core intensity exceeded inner core intensity (during t = 24~30h) and reached 45 m s^{-1} at t = 36h. TC size (Fig. 6c) increased during the size-growth period and remained unchanged during the intensification period, while the inner core strength (Fig. 6d) kept increasing throughout the simulation.

In Q- and QN-, TCs did not experience size-growth before intensification. The simulated inner core intensity kept increasing throughout the simulation period, and reached up to 65 m s^{-1} at t = 36h, which is much more intense than in CTRL. The outer core inten-

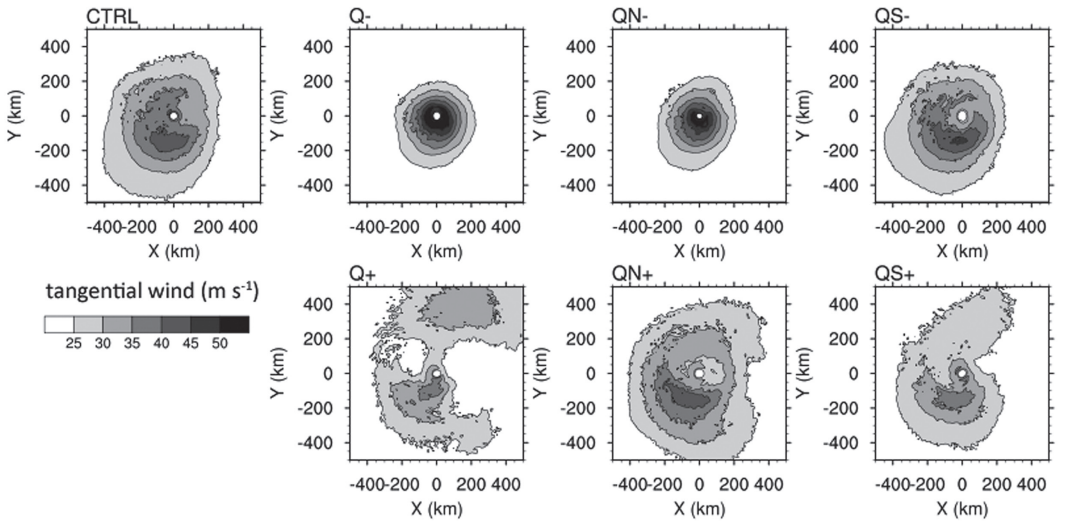

Fig. 5. Plane view of tangential wind speed at 1km height averaged over the intensification period for each run. Contours are drawn for 25~50 m s^{-1} levels with 5 m s^{-1} intervals. X and Y axes are the distance (km) from TC center.

sity never exceeded inner core intensity, and TC size remained small compared to CTRL. The inner core strength was stronger than CTRL. This indicates that TCs developed relatively small but intense vortices in drier environment (see vortex structure of QN- and Q- in Fig. 5).

For TCs in a moister environment (Q+, QN+ and QS+), the intensification rate for both the inner and outer core is lower than in CTRL. Their size kept increasing throughout the simulation period and their inner core strength increases much slower than CTRL. From their wind field structure (Fig. 5), we deduce that the moister environment yields TCs with loosely organized wind speed maxima in the outer core region. Compared to CTRL, TCs in Q+, QN+ and QS+ are larger in size and weaker in inner core strength.

Although the same amount of moisture was subtracted from model grid in QN- and QS-, they exhibits very different TC vortex behavior. TC vortex structure and intensity in QN- was similar to Q-, while QS- didn't deviate much from CTRL. This implies that the location of moisture, as well as the amount, plays an important role in altering the vortex structure and intensity of Typhoon Talim.

3.3 Propagation of outer rainband

Figure 7 displays the time evolution of radial distribution of azimuthal mean radar reflectivity and tangential wind speed at 1 km height. In CTRL, the size of TC wind field increased abruptly at t = 12h, with a secondary maximum of reflectivity (outer rainband convection) and tangential wind speed appearing at ~200 km radius and propagating radially inward. However, there is no clear separation between inner and outer radar reflectivity maxima. From the plane view of radar reflectivity (Fig. 3), we see that the outer rainband spirals inward into TC core and is connected with the eyewall. The radially inward propagation of convection in outer core region eventually merges with inner core eyewall convection during the intensification period.

For TCs in a drier environment (Q- and QN-), less convection is generated in the outer core region than in CTRL. The convection propagates more rapidly inward and merges with inner core convection. In the outer core region, no secondary maximum of tangential wind speed or radar reflectivity was forming. Instead, the inner core convection becomes stronger and tangential wind field extends radially outward, while the outer core region remains relatively radar echo-free. On the contrary, TCs in a moister environment (Q+, QN+ and QS+) developed more convection in the outer core. This convection at 200~300 km radii did not propagate radially inward as in CTRL. It kept rotating around TC in the outer core region, or even propagate outward slowly as TCs expand in tangential wind field extent.

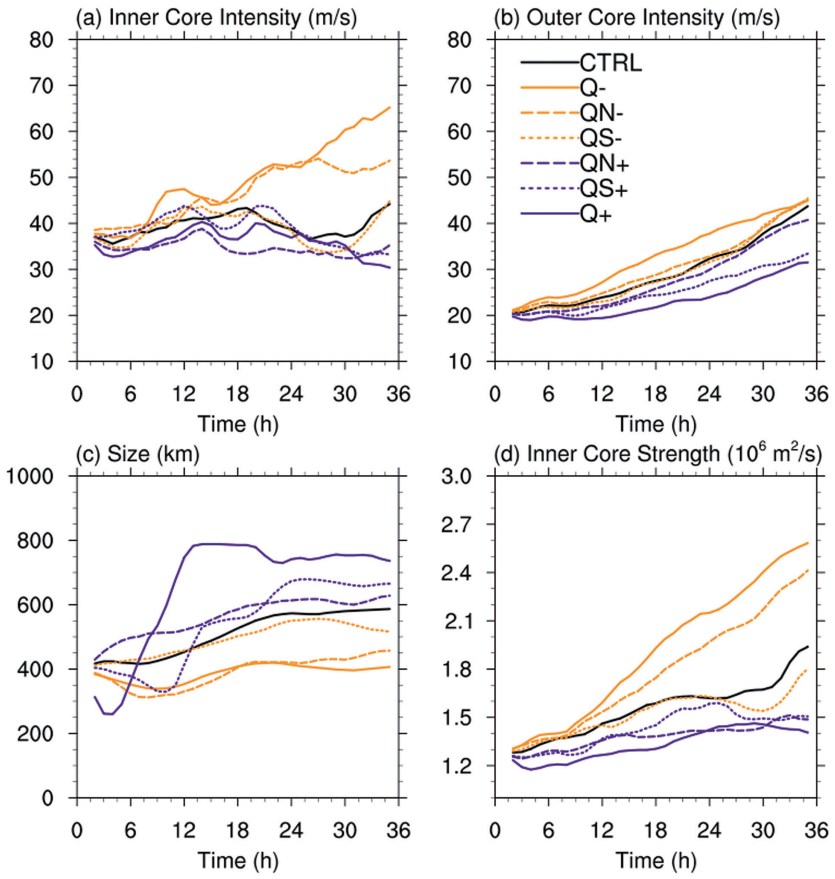

Fig. 6. Evolution of TC structural parameters for each run: (a) inner core intensity, (b) outer core intensity, (c) size and (d) inner core strength. We define inner core as region within r = 100km radius (including eyewall and inner rainbands), and outer core as the 100 km < r <300 km region. The inner and outer core intensity is the maximum tangential wind speed at z = 1 km found in each region. Size is defined as radius of gale force wind (azimuthal mean tangential wind speed exceeding 17 m s^{-1}), and inner core strength is the relative angular momentum averaged over inner core region.

3.4 Vertical structure

The vertical structure of the azimuthal mean TC primary and secondary circulations are shown in Figs. 8, 9, respectively. The primary circulation is also known as the tangential wind field (rotational wind), while the secondary circulation consists of the radial and vertical wind. During the intensification period of CTRL, rainbands in the outer core region are propagating radially inward to merge with the primary eyewall convection. The result is a radially broadened tangential wind field (see vertical section for CTRL in Fig. 8). As for the secondary circulation, Pendergrass and Willoughby (2009) proposed that diabatic heating in the eyewall induces updrafts within the heating and low-level inflow (upper-level outflow) beneath (atop) the heating. In our simulation, the location of diabatic heating and secondary circulation agrees well with their results. In CTRL, diabatic heating in the outer rainband extend throughout the outer core region in mid-level (z = 3~9km) (see CTRL in Fig. 9). The updraft induced by the diabatic heating tilts radially outward with height, and the mid-level inflow speed decreases with height. Maximum upward motion within the boundary layer occurred at ~200 km radius, that is also the radius closest to TC core that the mid- to low-level inflow layer could reach.

Compared with CTRL, TCs in Q- and QN- developed higher tangential wind speed with a smaller horizontal extent. The horizontal extent of 30 m s^{-1} azimuthal mean tangential wind in CTRL is about 300 km, but

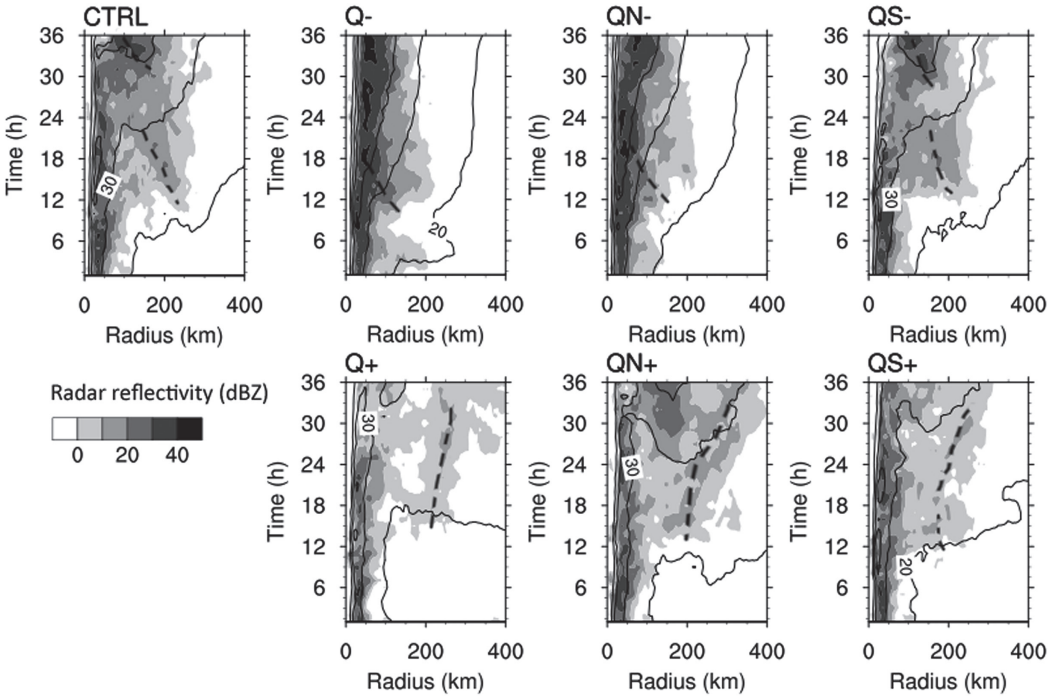

Fig. 7. Radius-time Hovmöller plots of azimuthal mean radar reflectivity and tangential wind speed at 1 km height for each run. Reflectivity shadings are at 0~40 dBZ levels with 10 dBZ intervals. Tangential wind contours are drawn for 20, 30 and 40 m s^{-1} levels. Thick dashed lines indicate the propagation of convection in outer core region.

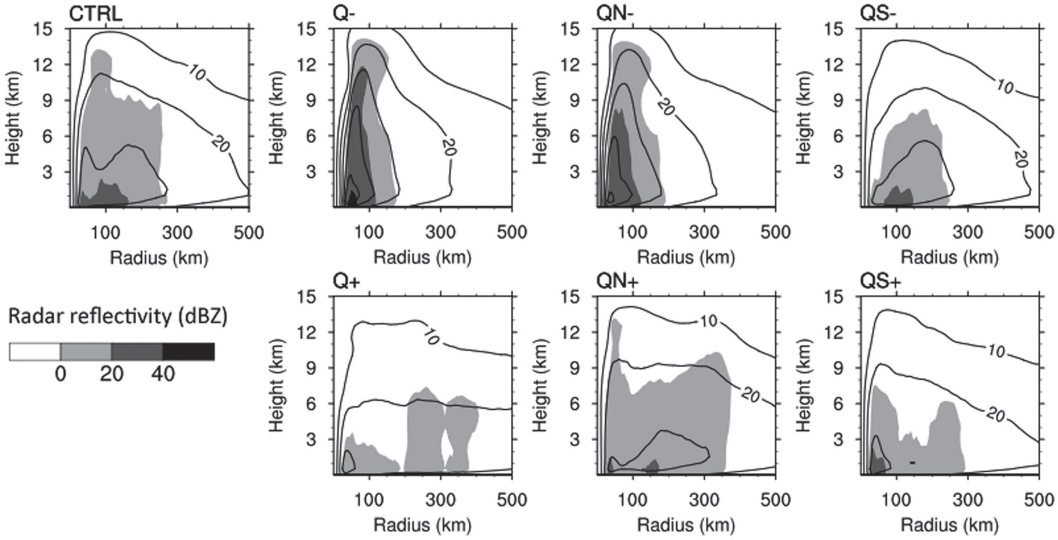

Fig. 8. Radius-height plots of the azimuthal mean radar reflectivity (shadings) and tangential wind speed (contours) averaged over the intensification period for each run. Reflectivity shadings are drawn for 0, 20 and 40 dBZ levels. Tangential wind contours are drawn for 10, 20, 30 and 40 m s^{-1} levels.

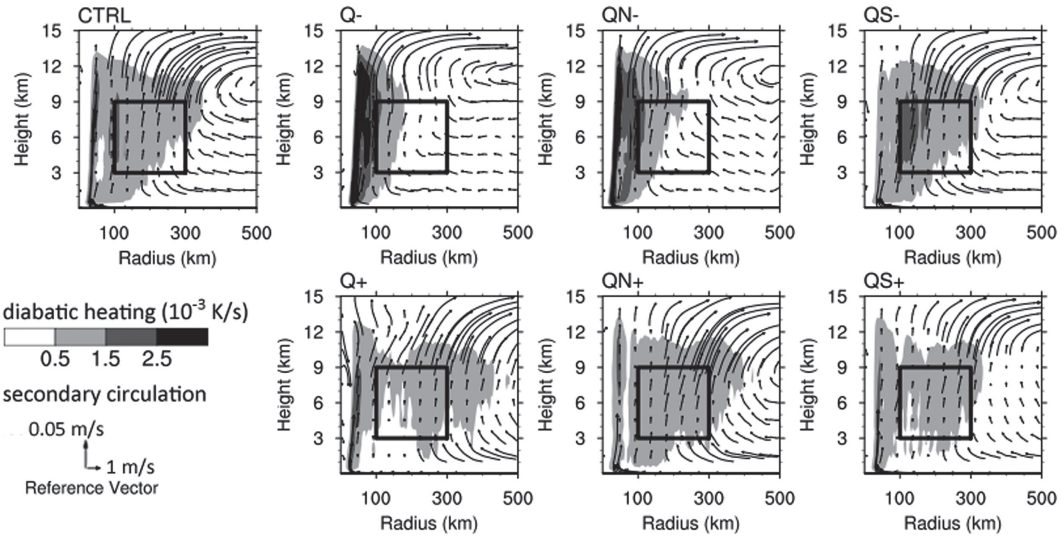

Fig. 9. Radius-height plots of diabatic heating rate (shadings) and secondary circulation (horizontal vectors for v_r and vertical vectors for w) averaged over the intensification period for each run. Diabatic heating rate shadings are drawn for 0.5, 1.5 and 2.5 $\times 10^{-3}$ K s^{-1} levels. Solid box indicate the mid-level outer core region.

only 200 km in Q- and QN-. A larger diabatic heating rate is found within the eyewall and inner rainbands, while in the outer core region, no diabatic heating is evident due to the lack of outer rainband convection. With this more radially concentrated heating, the mid- to low-level inflow reaches closer to the inner core region than in CTRL, and the updrafts in the boundary layer are near 100 km radius. The mid-level inflow layer also reaches into ~200 km radius, while in CTRL, the inflow slows down at ~300 km radius.

In case of a moister environment, Q+, QN+ and QS+ yielded TCs with shallower and broader tangential wind field than CTRL. The loosely organized convection in outer core region exerts latent heat throughout the outer core. The horizontal extent of diabatic heating in mid-level is even larger in Q+ than in CTRL. The resulting secondary circulation features a lack of inflow in the mid-level outer core region. Low-level inflow slows down underneath the rainband convection at ~100 km radius and tilts radially outward as uplifted and feed back into the rainband in mid-level (see QN+ in Fig. 9). Such overturning secondary circulation is consistent with the dynamic response of TC vortex to rainband diabatic heating as proposed by Moon and Nolan (2010).

4. Interpretation

4.1 Moisture's feedback on storm-relative flow

Before quantifying the contribution of rainband diabatic heating to TC structural change, it is necessary to first take a look at the storm-relative flow for each simulation since previous studies proposed that TC structure is susceptible to changes in the storm-relative flow (Wang and Holland 1996; Frank and Ritchie 2001). The evolution of vertical wind shear (defined as difference of storm-relative wind at 9 km and 3 km height averaged over 200km<r<600km area) is shown in Fig. 3. During the size-growth period, CTRL, Q-, QN-, QS- and QN+ developed weak easterly vertical wind shear (~1.8 m s^{-1} at t = 12h), while QS+ and Q+ developed relatively large southwesterly vertical wind shear (~3.6 m s^{-1} at t = 12h). For all runs, the outer rainbands are located initially in the northwest sector, which is the location (downshear) that favors enhancement of convection under a sheared condition (Wang and Holland 1996). In QS+ and Q+, the 3.6 m s^{-1} southwesterly shear appears to suppress the initial outer rainbands in northwestern sector. The initial outer rainband weakens and another rainband forms in the eastern sector of outer core during t = 12~24h. This behavior is different with other runs, as vertical shear direction does not change much in CTRL, Q-, QN-, QS- and QN+, the initial rainband kept quasi-stationary in the western sector throughout the 0~36h period.

In our experiments, the modification of TC moisture field leads to changes in storm-relative flow and vertical wind shear (Q+ and QS+). This indicates that moisture disturbances could exert impact on TC

structure indirectly through altering the storm-relative flow pattern. In the next sections, we will evaluate the contribution to TC structural changes by the latent heat released in outer rainband. Thus, only CTRL, Q-, QN- and QS- are analyzed because the storm-relative flows are similar among these runs. This allows us to rule out the influences from storm-relative flow to TC structural changes.

4.2 Sensitivity with regard to moisture amount

To quantify the contribution by diabatic heating induced secondary circulation to the intensification of TC rotational wind field, we performed a tangential wind budget analysis upon model simulation. The tangential wind budget equation in storm-relative cylindrical coordinates can be written as following (Xu and Wang 2010):

$$\frac{\partial \overline{v}_t}{\partial t} = -\overline{v}_r\overline{\eta} - \overline{v_r'\eta'} - \overline{w}\frac{\partial \overline{v}_t}{\partial z} - \overline{w'\frac{\partial v_t'}{\partial z}} + \overline{F_{sg}}$$

where t is time, z is height, v_t is tangential wind speed, v_r is radial wind speed, w is vertical velocity and η is the vertical component of absolute vorticity. $\overline{(\ )}$ designates azimuthal mean and $(\ )'$ designates azimuthal eddy terms. Five terms on the right hand side are radial advection of azimuthal mean absolute angular momentum by azimuthal mean radial wind (mean radial advection), radial advection by eddy process (eddy radial advection), vertical advection of azimuthal mean absolute angular momentum by azimuthal mean vertical motion (mean vertical advection), vertical advection by eddy process (eddy vertical advection) and friction and sub-grid mixing term (sub-grid forcing). The tendency of tangential wind and the first four terms on the right hand side are calculated directly from model simulated wind field, and the sub-grid forcing term is calculated by balancing the equation.

The radius-height plots for each term in the tangential wind budget averaged for the intensification period (t = 24~36h) are shown in Fig. 10 (CTRL) and Fig. 11 (Q-). In CTRL, the time tendency of azimuthal mean tangential wind speed (Fig. 10a) in the outer core is larger than in the inner core. The mean radial advection (Fig. 10c) contributes negatively to the increase of tangential wind speed in the mid-level outer core region, while the mean vertical advection contributes positively in the same region. The eddy terms (Figs. 10e, f) are small compared with azimuthal mean terms, but they are still not negligible. The sub-grid forcing term is negligible in the mid-level outer core region because friction and vertical mixing are relatively small in the mid-level free atmosphere.

A recent study on TC outer core spin-up process (Fudeyasu and Wang 2011) showed in their simulation that the radial and vertical advection of absolute angular momentum both contribute positively to the increase in tangential wind speed in TC outer core. However, in our simulation of Typhoon Talim (2005), the mean radial advection term contributes negatively to outer core tangential wind speed increase. TC simulated in their TCM4 model (Fudeyasu and Wang 2011) had a much smaller size than Typhoon Talim simulated in this study, the outer rainband extends only to 150 km radius in the mid-level. The outer core region of simulated Typhoon Talim is dominated by updrafts induced by the diabatic heating in outer rainbands (see CTRL in Fig. 9). These updrafts tilt radially outward slightly with height so that there is radially outward air motion that advects absolute angular momentum away from TC in the mid-level outer core, which explains the negative contribution by radial advection term in CTRL (Fig. 12c). Similar pattern of such negative mean radial advection can also be found in the inner core region of TC simulated in TCM4 (Fudeyasu and Wang 2011). As the outer core of Typhoon Talim is dominated by diabatic heating-induced updrafts, the major contribution to tangential wind speed increase is by vertical advection of low-level absolute angular momentum to the mid-level (see Fig. 12).

Comparing with CTRL, Q- has lower increasing rate in tangential wind speed in the mid-level outer core region. The tangential wind speed increases most rapidly in the inner core region (Fig. 11a). The negative contribution by radially outward advection of absolute angular momentum is compensated by the radially inward advection due to mid-level inflow that reached closer to the inner core (Fig. 11c). The net contribution of mean radial advection in outer core is close to zero (Fig. 12c).

The simulated azimuthal mean tangential wind speed changes in response to ambient moisture variations are consistent with previous ideal numerical experiments (Wang 2009; Hill and Lackmann 2009). Our results indicate that reducing TC environmental moisture causes TC to have lower (higher) increasing rate of outer (inner) core tangential wind speed in mid-level. Bister (2001) explained regarding the effect of peripheral convection on TC structure that the diabatic heating in rainbands lower the pressure of outer area and decreases the radial pressure gradient near TC core, and thus weakens the primary circulation. Our simulation verified his results. In the outer core region, the radial pressure gradient is larger in Q- than in CTRL (not shown). The increased pressure

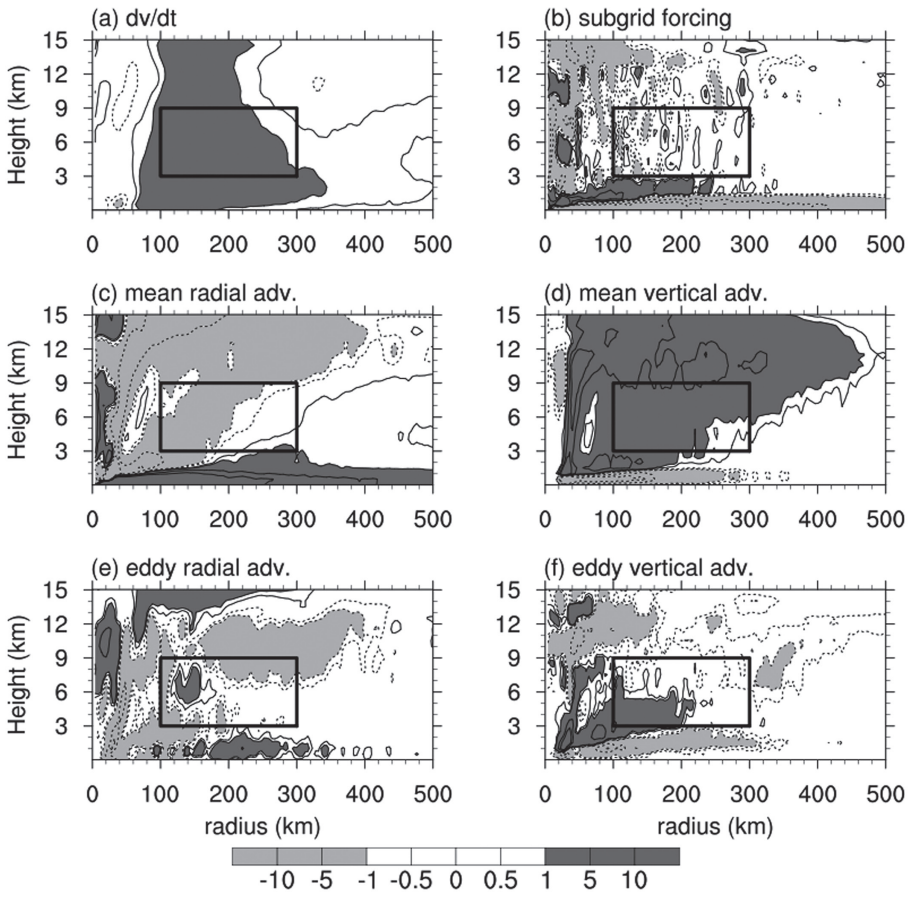

Fig. 10. Terms in the tangential wind budget equation averaged over the intensification period for CTRL run: (a) time tendency of azimuthal mean tangential wind speed, (b) sub-grid forcing terms including friction and vertical mixing, (c) mean radial advection, (d) mean vertical advection, (e) eddy radial advection and (f) eddy vertical advection. Contours are drawn for ±0.5, ±1, ±2, ±5 and ±10 $\times 10^{-4}$ m s^{-2} levels with negative values dashed. Values lower than -10^{-4} m s^{-2} are shaded with light gray and those higher than 10^{-4} m s^{-2} are shaded with dark gray. Solid box indicate the mid-level outer core region.

gradient could be associated with enhanced mid-level inflow that advects angular momentum radially inward into inner core.

4.3 Sensitivity with regard to moisture distribution

The different TC vortex behavior in QN- and QS- that we showed in Subsection 3.2 indicates that the TC structure is sensitive to the location of moisture. Subtracting the same amount of moisture from the southern sector (QS-) didn't produce the same result as QN-, which indicates that Typhoon Talim's vortex structure was influenced less by the reduction of moisture in the southern sector than in the northern sector. To understand this, backward trajectories were calculated for each run to determine the source location of peripheral air reaching TC inner core region (Fig. 13 shows results for CTRL). In CTRL, at the 600km radius, air from northwest and north takes about 15 hours to reach inner core, while air from south and southeast travels for more than 30 hours before it reaches inner core. This is also true in other runs (not shown). This explains why QN- yields a TC with suppressed outer rainband, while QS- still has a well-defined outer rainband. Although moisture is reduced in the southern sector, it takes twice the time for the drier air to influence the outer rainband in the west. When low-level dry air spirals into the rainband, it regains humidity by picking up moisture flux from ocean surface or through mixing with moister air in the north. Thus, the reduction of moisture in southern sector does not affect TC

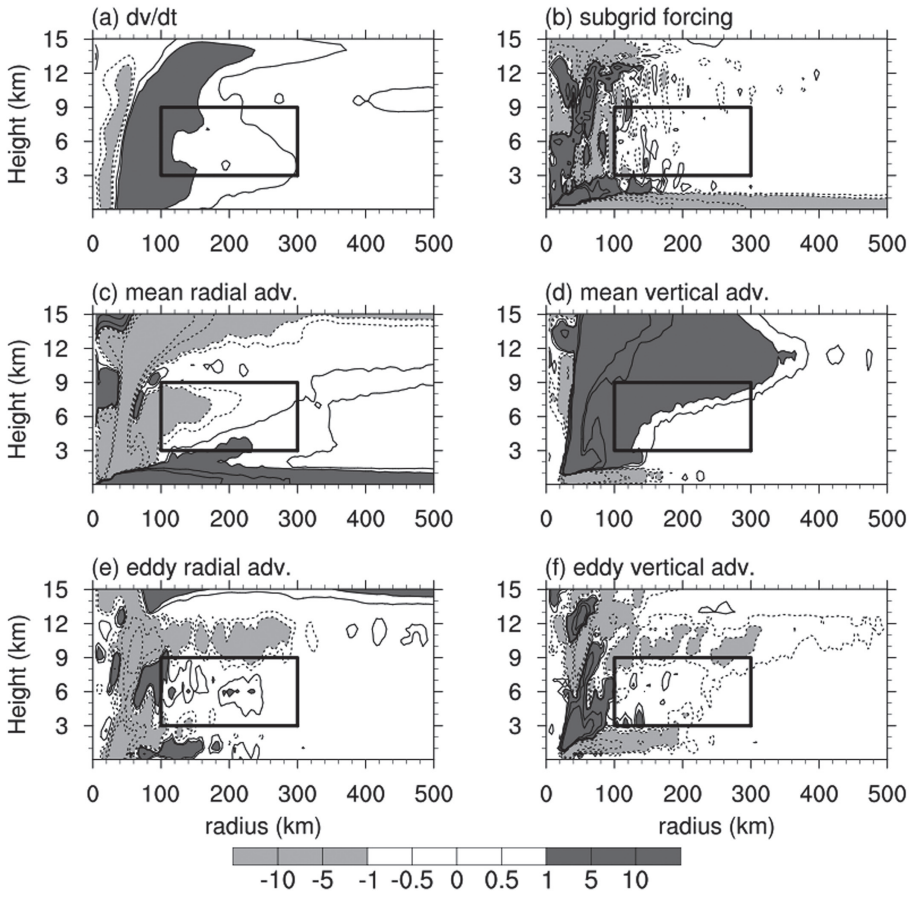

Fig. 11. Same as Fig. 10, but for Q- run.

outer rainband much.

From the tangential wind budget (Fig. 12), we found that, after the reduction of moisture in south (QS-), the contribution to outer core spin-up by each term remains almost the same as CTRL. Since the outer rainband is influenced little by such reduction of moisture, features related with rainband heating still remain unchanged. On the other hand, reduction of moisture in the north (QN-) produced almost the same result with reducing moisture throughout the model domain (Q-). This once again proved that, with the presence of shear-induced asymmetries, TC vortex structure is sensitive only to the moisture that feeds right into the rainband (air from the north in our case).

4.4 Interaction between outer core and inner core

In Subsection 3.3, we showed the different radial propagation speed of convection in outer core. In Q- and QN-, convection generated in the outer core move radially inward rapidly due to higher mid-level radial inflow speed. As we infer from the tangential wind budget, the lack of convectively generated updrafts in the outer core leads to smaller mean vertical advection (Fig. 12d). The increased mid-level radial inflow speed is a result of the relatively convection-free condition in outer core. In Q+, QN+ and QS+, convectively generated updrafts fill the outer core. Diabatic heating within the updraft induces low-level overturning secondary circulation that advects absolute angular momentum away from TC and also acts against the radial inward propagation of outer core convection.

The size-growth of Typhoon Talim could be viewed as the rapid generation of convection in the outer core, and as those convection organize into the outer rainband and propagate radially inward, the overturning flow on the inward side of outer rainbands (see CTRL in Fig. 9) causes the inner core eyewall and rainbands to expand and emerge with the outer rainbands (see

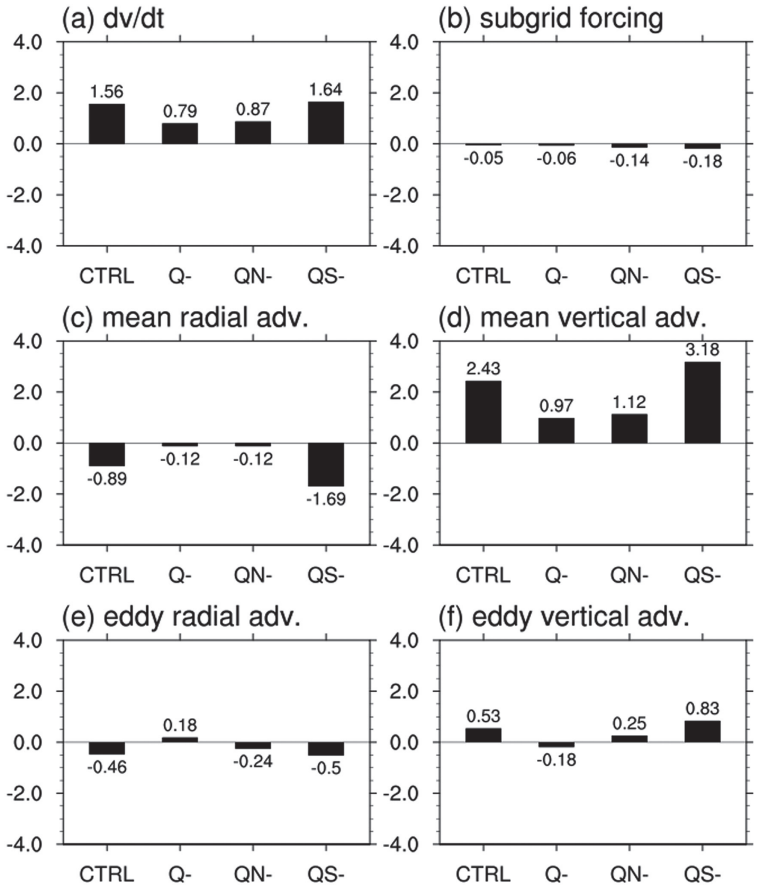

Fig. 12. Terms in the tangential wind budget equation averaged within the outer core region (box area in Fig. 10) over the intensification period for CTRL, Q-, QN- and QS-: (a) time tendency of azimuthal mean tangential wind speed, (b) sub-grid forcing terms including friction and diffusion, (c) mean radial advection, (d) mean vertical advection, (e) eddy radial advection and (f) eddy vertical advection. Terms are in units of 10^{-4} m s^{-2}.

CTRL in Fig. 7), while radial inflow on the outward side of the outer rainbands advects angular momentum into TC, spinning up the outer core. With reduced moisture in outer core (Q-), TC contract quickly due to enhanced mid-level inflow and the inner core strengthens faster than the outer core. On the other hand, when there is abundant moisture in outer core (Q+), convection generated there could block the radial inflow in the mid-level. Overturning secondary circulation in Q+ leads to a much slower emerging of inner and outer rainbands comparing with CTRL.

5. Summary and Discussion

Recent studies have shown that moisture plays an important role in altering TC vortex structure. In order to further explore the behavior of TC vortices in varying ambient moisture, we conducted sensitivity experiments with full physics cloud-resolving WRF simulations of Typhoon Talim (2005). In our simulations, TCs move westward with the presence of increasing vertical wind shear during its intensification period (t = 24~36h). TCs develop asymmetric outer rainbands that concentrate in the southwestern sector. With the presence of an easterly vertical wind shear, the outer rainbands are quasi-stationary and trajectory analysis showed that air from the north travels faster into TC inner core, compared to the air from the south. Thus, we modified the amount of moisture in the northern, southern sectors and in the whole domain to evaluate the sensitivity of TC structure with regard to both moisture amount and distribution.

Results showed that TC is sensitive to moisture variations in the northern sector, where air travels for only 15 hours to reach inner core. With sufficient moist air

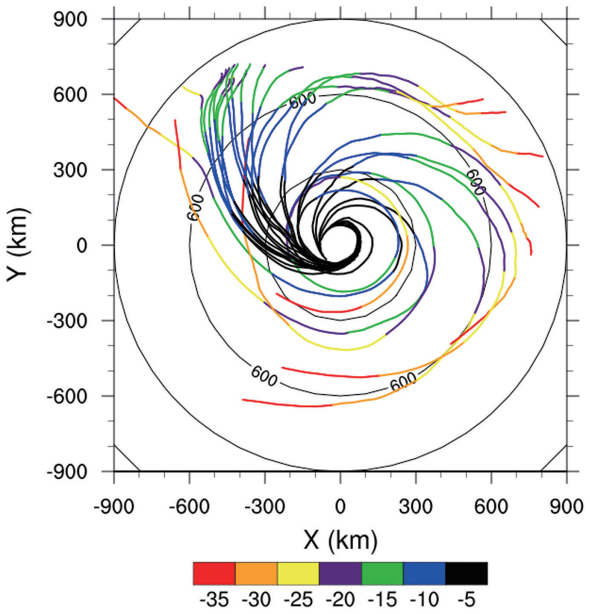

Fig. 13. Backward trajectories at z = 1km level seeded along r = 100 km radius (the outer boundary of inner core). The colors denote the time (hour) of backward integration. For example, blue lines indicate location of air reaching the inner core region after 10 hours. Radii of 300, 600 and 900 km are drawn in thin black lines.

from the north, TC develops more convection in outer core region. Strong outer rainbands release latent heat in the outer core region, which enhances updrafts and reduces mid-level radial inflow. The reduced inflow suppresses the radial advection of absolute angular momentum into the inner core, thus the inner core intensity decreases. On the other hand, with drier air intruding into the inner core from the north, convection in TC the outer core region is suppressed. The convection-free outer core region provides favorable mid- to low-level radial inflow that speeds up the inner core spin-up process. In case of outer rainbands with sufficient upstream moisture supply, the reduced radial inflow speed causes the convection to stay in the outer core region throughout the simulated period, which yields larger TC size. However, in case of suppressed outer rainbands due to drier air intrusion, the convection generated in outer core region is advected radially inward by the enhanced mid- to low-level inflow, and this causes TC to contract and have smaller size.

Combining our results with findings from idealized simulations in previous studies (Wang 2009; Hill and Lackmann 2009), we summarize the responses of TC vortex structure to ambient moisture variations as schematic diagrams in Fig. 14. In idealized TCs, the ambient flow is not sheared and TCs develop symmetric structures. Moister environment yields TCs with expanded cores, often associated with the breakdown of eyewall (Fig. 14a). In a drier environment, TCs will contract due to enhanced secondary circulation, and grow smaller in size with less outer rainband convection (Fig. 14b). TCs in drier environment intensify faster and have a shorter life cycle than those in a moister environment. In a sheared environment, TCs develop asymmetric outer rainbands, and only the moisture from the upstream side of TC rainbands exerts a significant impact on TC structure. Provided sufficient moisture supply (Fig. 14c), the outer rainbands will grow stronger and latent heat released in outer rainbands induces upward motion reducing the radial inward advection of absolute angular momentum, which weakens the inner core intensity. On the contrary, drier upstream inflow to the outer rainbands (Fig. 14d) inhibits convection and yields small TCs with strong inner core intensity and strength.

Although Typhoon Talim (2005) had a typical life cycle of West Pacific typhoons, the ambient flow evolution could be quite unique with regard to each TC case. For example, some TCs could experience much larger vertical wind shear in their early development stage and will not have the chance to reach their mature stage. Some TCs could experience vertical wind shear with decreasing magnitude during their mature stage, which may yield different results from our experiments. In order to fully understand the mechanism of TC structural change in response of ambient moisture variations, further experiments should be conducted regarding different environmental conditions from our case. Nevertheless, our sensitivity experiments gave inspiring results that TC wind field structure is quite sensitive to ambient moisture content and distribution. The role of moisture in TC evolution is quite important, and should still be one of the key factors of TC structural changes in further studies.

Acknowledgements

We appreciate the comments from two anonymous reviewers of this study. We would also like to thank Dr. Yuqing Wang from University of Hawaii and Dr. Hung-Chi Kuo from National Taiwan University for their valuable discussion and comments on this paper. This study is supported by National Basic Research Program of China (Grant No. 2009CB421504), Chinese National Science Foundation under Grants

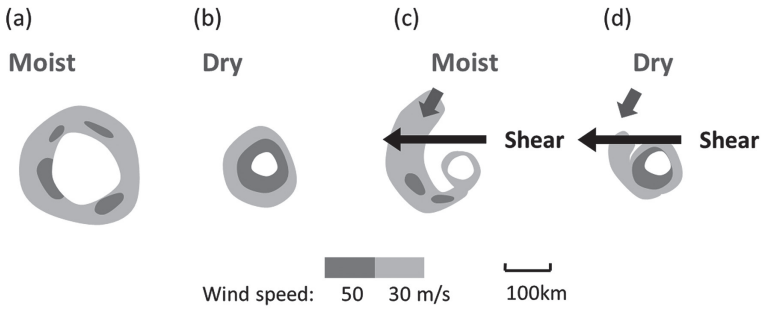

Fig. 14. Schematic diagrams showing TC wind field structure associated with ambient moisture configuration. In case of axi-symmetric TCs, moister environment yields expanded TC wind field (a), while drier environment causes TC to contract (b). For TCs with shear-induced asymmetric rainbands, rainband convection is sensitive to moisture supply from the upstream side. More moisture supply yields stronger rainband convection and wind gusts inside rainbands could exceed core intensity (c), while less moisture supply inhibits rainband convection and these convection contribute to core intensity during axi-symmetrization (d).

41275048 and 40921160380, and GYHY 201006011. We also thank the WRF community for providing and maintaining the software.

References

Atangan, J. F., and A. Preble, 2006: *2005 Annual Tropical Cyclone Report*. US Naval Pacific Meteorology and Oceanography Center/Joint Typhoon Warning Center, Pearl Harbor, Hawaii, USA., https://metoc.npmoc.navy.mil/jtwc/atcr/2005atcr/.

Bister, M., 2001: Effect of Peripheral Convection on Tropical Cyclone Formation. *J. Atmos. Sci.*, **58**, 3463–3476.

Braun, S. A., 2010: Reevaluating the Role of the Saharan Air Layer in Atlantic Tropical Cyclogenesis and Evolution. *Mon. Wea. Rev.*, **138**, 2007–2037.

Corbosiero, K. L., and J. Molinari, 2002: The Effects of Vertical Wind Shear on the Distribution of Convection in Tropical Cyclones. *Mon. Wea. Rev.*, **130**, 2110–2123.

Dudhia, J., 1989: Numerical study of convection observed during the winter monsoon experiment using a mesoscale two-dimensional model. *J. Atmos. Sci.*, **46**, 3077–3107.

Elsner, J. B., J. P. Kossin, and T. H. Jagger, 2008: The increasing intensity of the strongest tropical cyclones. *Nature*, **455**, 92–95.

Emanuel, K. A., J. David Neelin, and C. S. Bretherton, 1994: On large-scale circulations in convecting atmospheres. *Quart. J. Roy. Meteor. Soc.*, **120**, 1111–1143.

Frank, W. M., and E. A. Ritchie, 2001: Effects of Vertical Wind Shear on the Intensity and Structure of Numerically Simulated Hurricanes. *Mon. Wea. Rev.*, **129**, 2249–2269.

Fudeyasu, H., and Y. Wang, 2011: Balanced Contribution to the Intensification of a Tropical Cyclone Simulated in TCM4: Outer-Core Spinup Process. *J. Atmos. Sci.*, **68**, 430–449.

Hendricks, E. A., M. S. Peng, F. Bing, and L. Tim, 2010: Quantifying Environmental Control on Tropical Cyclone Intensity Change. *Mon. Wea. Rev.*, **138**, 3243–3271.

Heymsfield, G. M., J. Simpson, J. Halverson, L. Tian, E. Ritchie, and J. Molinari, 2006: Structure of Highly Sheared Tropical Storm Chantal during CAMEX-4. *J. Atmos. Sci.*, **63**, 268–287.

Hill, K. A., and G. M. Lackmann, 2009: Influence of Environmental Humidity on Tropical Cyclone Size. *Mon. Wea. Rev.*, **137**, 3294–3315.

Holland, G. J., and R. T. Merrill, 1984: On the dynamics of tropical cyclone structural changes. *Quart. J. Roy. Meteor. Soc.*, **110**, 723–745.

Hong, S. Y., and J. O. Lim, 2006: The WRF single-moment 6-class microphysics scheme (WSM6). *J. Korean Meteor. Soc*, **42**, 129–151.

Hong, S.-Y., Y. Noh, and J. Dudhia, 2011: A New Vertical Diffusion Package with an Explicit Treatment of Entrainment Processes. *Mon. Wea. Rev.*, **134**, 2318–2341.

Kimball, S. K., 2006: A Modeling Study of Hurricane Landfall in a Dry Environment. *Mon. Wea. Rev.*, **134**, 1901–1918.

Lonfat, M., F. D. Marks, and S. S. Chen, 2004: Precipitation Distribution in Tropical Cyclones Using the Tropical Rainfall Measuring Mission (TRMM) Microwave Imager: A Global Perspective. *Mon. Wea. Rev.*, **132**, 1645–1660.

Low-Nam, S., and C. Davis, 2001: Development of a tropical cyclone bogussing scheme for the MM5 system. Preprint, *The Eleventh PSU/NCAR Mesoscale Model Users' Workshop, June*, 25–27.

Mlawer, E. J., S. J. Taubman, P. D. Brown, M. J. Iacono,

and S. A. Clough, 1997: Radiative transfer for inhomogeneous atmospheres: RRTM, a validated correlated-k model for the longwave. *J. Geophys. Res.*, **102**, 16663–16682.

Moon, Y., and D. S. Nolan, 2010: The Dynamic Response of the Hurricane Wind Field to Spiral Rainband Heating. *J. Atmos. Sci.*, **67**, 1779–1805.

Pendergrass, A. G., and H. E. Willoughby, 2009: Diabatically Induced Secondary Flows in Tropical Cyclones. Part I: Quasi-Steady Forcing. *Mon. Wea. Rev.*, **137**, 805–821.

Riemer, M., and M. T. Montgomery, 2011: Simple kinematic models for the environmental interaction of tropical cyclones in vertical wind shear. *Atmos. Chem. Phys.*, **11**, 9395–9414.

Wang, Y., 2009: How Do Outer Spiral Rainbands Affect Tropical Cyclone Structure and Intensity? *J. Atmos. Sci.*, **66**, 1250–1273.

Wang, Y., and G. J. Holland, 1996: Tropical Cyclone Motion and Evolution in Vertical Shear. *J. Atmos. Sci.*, **53**, 3313–3332.

Xu, J., and Y. Wang, 2010: Sensitivity of Tropical Cyclone Inner-Core Size and Intensity to the Radial Distribution of Surface Entropy Flux. *J. Atmos. Sci.*, **67**, 1831–1852.